ARID ZONE JOURNAL OF ENGINEERING, TECHNOLOGY & ENVIRONMENT
AZOJETE June 2026. Vol.22(2):274-288
Published by the Faculty of Engineering, University of Maiduguri, Maiduguri, Nigeria.
Print ISSN: 1596-2490, Electronic ISSN: 2545-5818
https://doi.org/10.63958/AZOJETE/2026/22/02/007
www.azojete.com.ng

DEVELOPMENT

DESIGN AND FABRICATION OF A COMBINED CHARCOAL GRINDING AND MOULDING MACHINE

I. Sulaiman*, V. N. Haruna, O. I. Enock

Department of Mechanical Engineering Department, The Federal Polytechnic Bida, Niger State
**Corresponding Author: skishk2009@gmail.com*

ARTICLE INFORMATION

Received: 16th February 2026
Revised: 7th March 2026
Accepted: 7th March 2026

Keywords:
Binder mixing
Biomass processing
Compaction
Design analyses
Performance

ABSTRACT

The design and fabrication of an affordable biomass processing equipment remain essential for improving small-scale charcoal briquette production in developing regions. This study presents the development and performance evaluation of a combined charcoal grinding, mixing, and moulding machine that integrates size reduction, binder mixing, and compaction into a single system to improve process efficiency and reduce losses. The machine was constructed primarily from mild steel and powered by a 2.2 kW electric motor. Design analyses were carried out to determine the power requirement, shaft dimensions, and mixing chamber capacity. Performance testing was carried out using 10 kg batches of dried charcoal and grinding times used ranged from 11.8 to 12.4 min. The results showed that the total power required by the machine was 1.185 kW, the calculated shaft diameter was 15 mm, while the mixing chamber capacity was 12.1 kg of charcoal mixture. Throughputs between 46.9 and 48.8 kg/h was obtained along with an average of 48.0 kg/h, corresponding to a capacity efficiency of 96.1% relative to the 50 kg/h design target. The moulding unit produced briquettes with uniform dimensions, having an average diameter of 40 mm, height of 35 mm, and mass of 85 g, indicating consistent compaction. Durability evaluation produced an average shatter index of 6.93%, indicating good resistance to breakage during handling and transportation, while combustion testing gave an average ignition rate of 8.04 mm/min, indicating stable flame propagation suitable for domestic cooking applications. The close agreement between experimental and design values demonstrates that the integrated machine operates efficiently and reliably. The developed system offers a simple and effective solution for small-scale conversion of charcoal fines and agricultural residues into densified solid fuel.

1.0 Introduction

Across many parts of the world, particularly in developing regions, increasing pressure on conventional energy sources coincides with the large-scale generation of agricultural residues such as rice husk, maize cobs, groundnut shells, coconut shells, and sawdust. Although often treated as waste, these materials contain considerable stored energy (Lackner and Besharati, 2025; Adeleke *et al*., 2021). Their disposal through open burning or natural decomposition contributes to environmental pollution, making their conversion into useful fuel both an energy and waste management solution (Maqsood *et al*., 2025).

One effective approach to valorising these residues is their conversion into densified charcoal fuels. In their raw form, charcoal fines are dusty, bulky, and difficult to handle, but densification into pellets or briquettes improves uniformity, handling, storage, and combustion performance (Sithole *et al*., 2023; Yan *et al*., 2015). This process enhances the physical integrity of biomass fuels and makes them more suitable for domestic and small-scale industrial applications.

The production of quality charcoal briquettes involves grinding, mixing with a binder, and moulding. After carbonisation, the charcoal must be reduced to fine, uniform particles commonly using hammer mills due to their simplicity and adaptability (Oyelami and Oluwole, 2023; Bassey *et al*., 2022; Gil and Arauzo, 2014; Adejugbe *et al*., 2023; Mugabi *et al*., 2019). Particle size uniformity at this stage is critical for effective binder interaction and compaction. The mixing stage is equally important, as proper binder distribution determines the mechanical strength and combustion consistency of the final product (Li *et al*., 2019; Sithole *et al*., 2023).

In most small-scale production systems, however, grinding, mixing, and moulding are carried out using separate machines. This fragmented arrangement increases labour, processing time, energy consumption, and material losses during handling. It also leads to higher power demand (typically about 1.5–2.2 kW for grinding and 1.5–3.0 kW for mixing) and greater equipment costs and space requirements due to the use of independent units (Adetola *et al*., 2022; Vodounnou *et al*., 2022; Ajayi *et al*., 2019; Dermawan *et al*., 2025; Adebukola and Patrick, 2019).

Despite these limitations, most existing studies have focused on individual components such as grinders or briquetting units, with limited attention to integrated systems. The absence of compact, multi-functional equipment reduces production efficiency and limits the adoption of briquette production technologies in resource-constrained settings. This study therefore presents the design, fabrication, and performance evaluation of an integrated charcoal grinding, mixing, and moulding machine for small-scale biomass processing. By combining these operations within a single unit, the system aims to improve efficiency, reduce energy and labour requirements, and enhance the quality of briquettes produced from agricultural residues.

2. Materials and Method

2.1 Materials

Mild steel of grade A36 was used for the machine frame, grinding chamber, mixing chamber, and moulding unit because of its good weldability, adequate strength, and wide availability. Typical mechanical properties of A36 mild steel include a yield strength of about 250 MPa, ultimate tensile strength of 400–550 MPa, Young's modulus of approximately 200 GPa, and elongation at break of about 20%, which makes it suitable for structural fabrication and moderate load-bearing components (Mishra *et al*., 2017). Steel angle bars and flat bars provided structural support and stability during operation (Figure 1).

The shaft and hammers were fabricated from medium-carbon steel (AISI 1045) to withstand repeated impact loads during grinding. This material typically possesses an ultimate tensile strength of about 570–700 MPa and good fatigue resistance, which improves durability during continuous operation (Irechukwu *et al*., 2025). Ball bearings were used to support the rotating shaft and reduce friction. A perforated steel plate served as the grinding screen to control particle size, while bolts and nuts were used for assembly and ease of maintenance.

Charcoal produced from carbonised agricultural residues was used as the primary raw material. The charcoal was obtained in lump form and sun-dried prior to processing to reduce moisture content. The moisture content of the charcoal before grinding was maintained at approximately 8% (wet basis) to improve grinding efficiency and briquette formation.

A starch-based binder (cassava starch) was used to enhance cohesion during moulding because of its low cost, local availability, and effectiveness in briquette production. The binder was prepared by dissolving starch in water at a concentration of about 5% as suggested by Lomunyak *et al*. (2024) and Aliero *et al*. (2022). The prepared binder was then mixed thoroughly with the milled charcoal to obtain a homogeneous briquetting mixture during the testing of the machine. A starch-to-charcoal ratio of approximately 1:19 (5% binder by weight) was used to ensure adequate binding strength without significantly affecting the combustion properties of the briquettes.

2.2 Design Analysis of the Hammer Mill Section

For small-scale operation, the capacity of the hammer mill was assumed as 50 kg/h. This capacity is suitable for cottage-level charcoal pellet production and allows for manual feeding and intermittent operation.

Corresponding author's email address: skishk2009@gmail.com

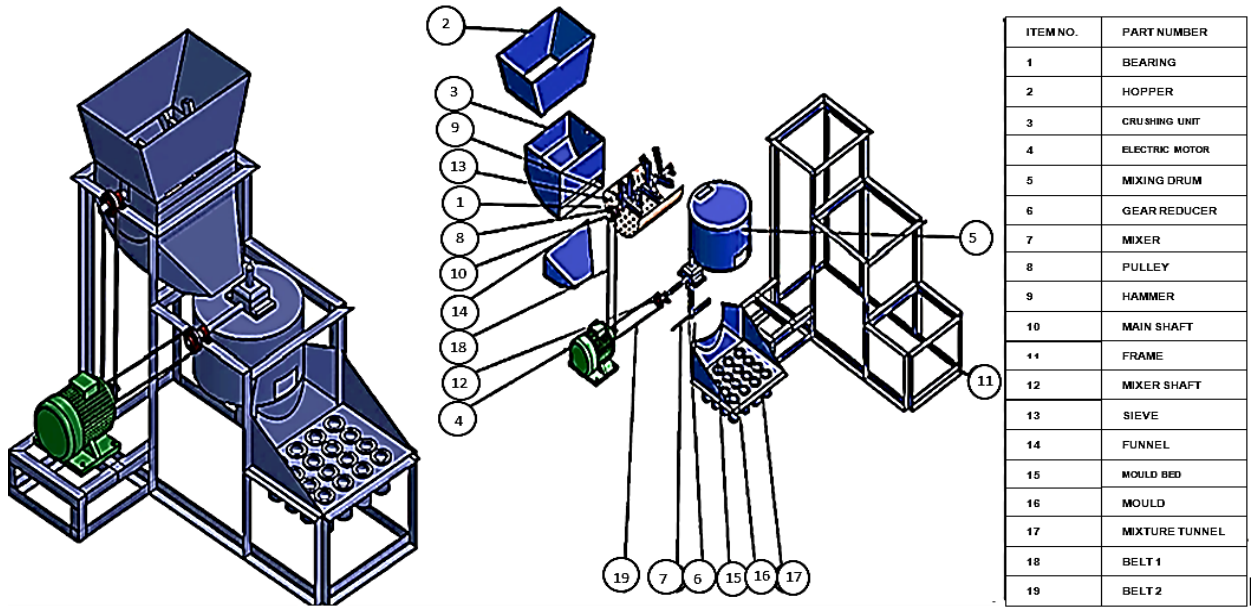

ITEM NO.	PART NUMBER
1	BEARING
2	HOPPER
3	CRUSHING UNIT
4	ELECTRIC MOTOR
5	MIXING DRUM
6	GEAR REDUCER
7	MIXER
8	PULLEY
9	HAMMER
10	MAIN SHAFT
11	FRAME
12	MIXER SHAFT
13	SIEVE
14	FUNNEL
15	MOULD BED
16	MOULD
17	MIXTURE TUNNEL
18	BELT 1
19	BELT 2

Figure 1: Working drawing of the machine

2.2.1 Determination of power requirement

The power required for grinding charcoal was estimated using the relationship between mass flow rate and specific energy requirement. For brittle materials such as charcoal, a specific energy requirement of approximately 12–15 kWh/tonne is commonly adopted (Sulaiman *et al*., 2021; Rhodes, 2008). A conservative value of 15 kWh/tonne was selected. Hence, Equation 1 was used to calculate the power required for the hammermill (Sulaiman *et al*., 2021).

$$P = E \times \dot{m} \quad (1)$$

Where P is the power required (W), E is the specific energy requirement (kWh/tonne) and $\dot{m}$ is the mass flow rate (tonne/h). for a 50 kg/h the $\dot{m}$ is 0.05 tonne/h.

$P = 15 \times 0.05 = 0.75$ kW
Applying a service factor of 1.3 to account for mechanical losses and shock loads (Sulaiman *et al*., 2021):

$P_d = 1.3 \times 0.75 = 0.98$ kW
where P_d is the design power for the hammermill.

2.2.2 Design of speed and pulley design

The electric motor speed is 2800 rpm, while suggested hammer mill rotor speed is 1800 rpm (Rhodes, 2008). The selected motor pulley diameter based on calculated power requirement is 80 mm. Equation 2 was used to determine the rotor pulley diameter.

$$N_1 D_1 = N_2 D_2 \quad (2)$$

where N_1 is the electric motor speed (rpm), D_1 is the diameter of the motor pully (m), N_2 is the hammer rotor speed (rpm) and D_2 is the diameter of the rotor pulley (m).

$2800 \times 0.08 = 1800 \times D_2$
$224 = 1800 \times D_2$
$D_2 = \frac{224}{1800}$
$D_2 = 0.124$ m or 124 mm

2.2.3 Determination of torque due to charcoal load on the hammer mill shaft

During operation, a portion of the charcoal is subjected to impact by the rotating hammers. The resisting torque on the shaft can be estimated by considering the weight of the charcoal being acted upon. The

Corresponding author's email address: skishk2009@gmail.com

instantaneous mass of charcoal impacted by the hammers was estimated as 0.85 kg based on the effective volume of material present in the grinding zone at a given time. The hopper and feed throat were designed such that only a limited quantity of charcoal is allowed into the grinding chamber during operation.

Considering the approximate feed chamber volume interacting with the hammer path (about 0.005 m³) and the bulk density of crushed charcoal is 200 kg/m³ according to Wasfy and Awny (2020), the mass of charcoal present within the hammer impact region at a given instant is estimated as the product of density and volume.

This value therefore represents the instantaneous mass of charcoal subjected to hammer impact during grinding, which was used in the torque calculation. The effective radius from the shaft centre to the point of impact is 0.23 m. Therefore, the force acting on the shaft is given by Equation (3).

$$F = mg \quad (3)$$

Where F is the force (N), m is the mass of the charcoal (kg) and g is the acceleration due to gravity (m/s²)

$F = 0.85 \times 9.81$
$F = 8.34$ N
The resisting torque on the shaft is given by Equation 4 (Sulaiman *et al.*, 2021):

$$T = Fr_{eff} \quad (4)$$

Where T is the torque (Nm) and r_{eff} is the effective radius (m).
$T = 8.34 \times 0.23$
$T = 1.92$ Nm

2.2.4 Determination of shaft diameter

The hammer mill shaft is subjected to combined torsion (from impact on the hammers) and bending (from the weight of the hammers and pulley loads as shown in Figure 2). The shaft diameter was designed using Equation 5 (Sulaiman *et al.*, 2021).

$$d^3 = \frac{16}{\pi\tau}\sqrt{(K_t T)^2 + (K_b M)^2} \quad (5)$$

Where d is the shaft diameter (m), τ is the allowable shear stress (Pa), K_t is the shock/fatigue factor for torsion, K_b is the shock/fatigue factor for bending and M is the bending moment on the shaft (N·m). Allowable shear stress for mild steel is suggested to be 40 MPa according to Sulaiman *et al.* (2021). The shock and fatigue factors K_t and K_b are 1.5 and 2.0 respectively.

The hammer mass was calculated from its volume and density. Assuming mild steel density $\rho = 7850$ kg/m³ (Sulaiman *et al.*, 2021). The hammer dimensions are 0.23 m $\times$ 0.05 m $\times$ 0.005 m. The volume and mass and weight of the hammers are obtained using Equations 6, 7 and 8 respectively.

$$V_{\text{hammer}} = L_{\text{hammer}} \times Wi_{\text{hammer}} \times H_{\text{hammer}} \quad (6)$$

$$m_{\text{hammer}} = \rho_{\text{hammer}} \times V_{\text{hammer}} \quad (7)$$

$$W_{\text{hammer}} = m_{\text{hammer}} g \quad (8)$$

Where V_{hammer} is the hammer volume (m³), L_{hammer} is the hammer length (m), Wi_{hammer} is the hammer width (m), H_{hammer} is the hammer height (m), m_{hammer} is the mass of the hammer (kg), ρ_{hammer} the density of the hammer (kg/m³), W_{hammer} is the hammer weight and g is the acceleration due to gravity (m/s²).

$V_{\text{hammer}} = L \times W \times H = 0.23 \times 0.05 \times 0.005 = 5.75 \times 10^{-5}$ m³
$m_{\text{hammer}} = \rho \times \text{Volume} = 7850 \times 5.75 \times 10^{-5} \approx 0.45$ kg
$W_{\text{hammer}} = mg = 0.45 \times 9.81 \approx 4.41$ N

Corresponding author's email address: skishk2009@gmail.com

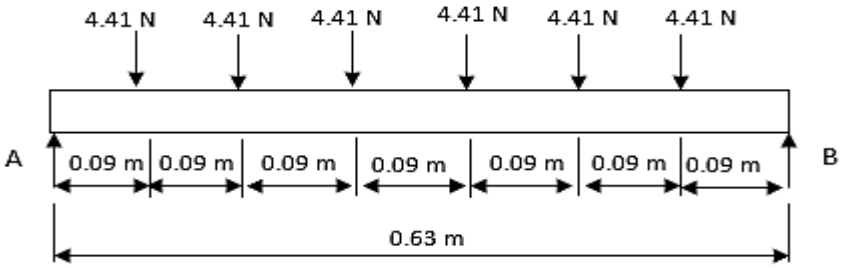

Figure 2: Free body diagram of the hammermill shaft

The total load on shaft (W_T in N) is the sum of all the hammer weights (in Figure 2), obtained as 26.46 N. Because the loading is symmetrical Equation 9 is true.

$$R_A = R_B = \frac{W_T}{2} \quad 9$$

Where R_A is the reaction at point A (N), R_B is the reaction at point B (N).

$R_A = R_B = 13.23$ N

For shear force calculation, the shear force exhibits a stepwise reduction of 4.41 N at each load location, beginning with $+13.23$ N at support A and reducing to 0 at midspan (0.27 m), after which it becomes negative and reaches -13.23 N just before support B. The maximum shear force magnitude is therefore: $V_{\max} = 13.23$ N.

For the bending moment calculation

Hammer positions from support A; $x = 0.09, 0.18, 0.27, 0.36, 0.45, 0.54$ m

The maximum bending moment occurs at midspan (between the 3rd and 4th hammers in Figure 2).

$x = \frac{L}{2} = 0.315$ m

Taking moments about support A:

$$M_{\max} = R_A x - \sum(W_i \times L_i) \quad 10$$

where $M_{\max}$is the maximum bending moment acting on the shaft (N·m), x is the distance from support A to the section under consideration (m), W_i is the concentrated load due to the i-th hammer (N), and L_i is the perpendicular distance from the point of application of each load to the section under consideration (m).

Loads to the left of midspan are the first three hammers, with distances from midspan obtained as 0.045 m, 0.135 m and 0.225 m respectively.

$0.315 - 0.27 = 0.045$m
$0.315 - 0.18 = 0.135$m
$0.315 - 0.09 = 0.225$m

$M_{\max} = 13.23(0.315) - 4.41(0.045 + 0.135 + 0.225)$
$M_{\max} = 4.17 - 4.41(0.405)$
$M_{\max} = 4.17 - 1.79 = 2.38$ Nm

The shear force and bending moment diagram is given in Figure 3.

The values calculated were then substituted into Equation 5.

Corresponding author's email address: skishk2009@gmail.com

$$d^3 = \frac{16}{\pi(40\times10^6)}\sqrt{(1.5\times1.92)^2 + (2\times2.38)^2}$$
$$= \frac{16}{125.66\times10^6}\sqrt{(2.88)^2 + (4.76)^2}$$
$$= 1.273\times10^{-7}\times\sqrt{8.29 + 22.66}$$
$$= 1.273\times10^{-7}\times5.56$$
$$d^3 = 7.08\times10^{-7}$$
$$d = 0.0089\ \text{m} = 8.9\ \text{mm}$$

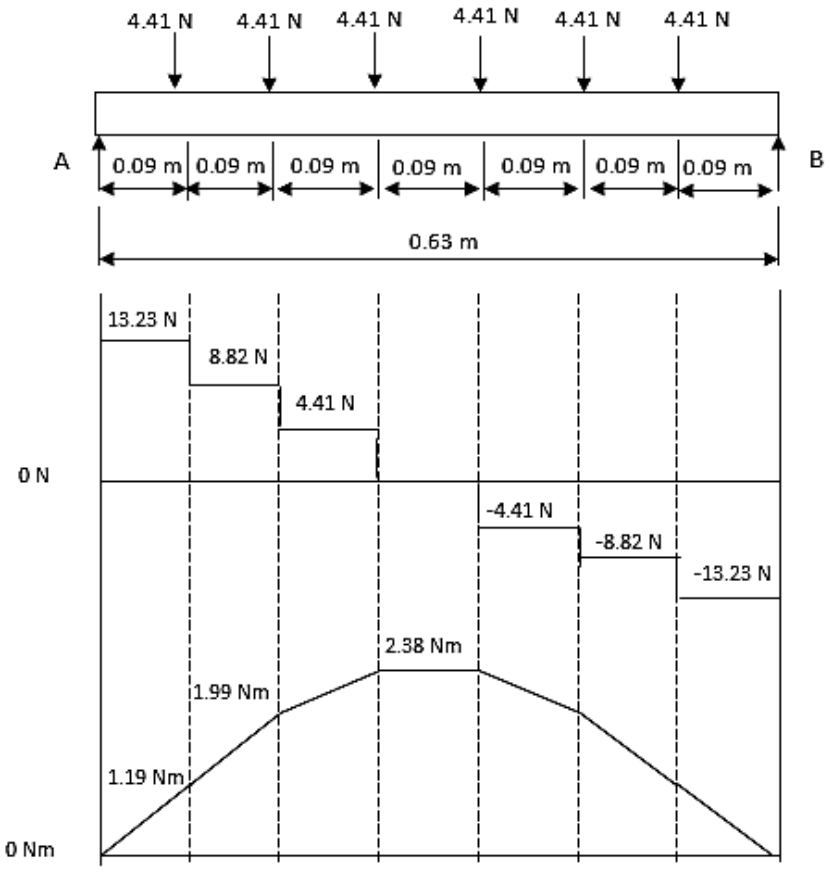

Figure 3: Shear force and bending moment diagrams for the hammer mill shaft

The calculated minimum shaft diameter is 8.9 mm. Considering shock loading, manufacturing tolerances, and safety, the available standard shaft diameter of 15 mm was considered safe for the hammer mill unit.

2.2.5 Design and selection of bearing

Since the calculated shaft diameter was 15 mm, a 6202 deep groove ball bearing with an inner bore diameter of 15 mm, outer diameter of 35 mm, and width of 11 mm was selected. Deep groove ball bearings were preferred because they are capable of supporting moderate radial loads while operating at relatively high rotational speeds (Budynas and Nisbett, 2015).

2.3 Design Analysis of the Mixing Chamber

The mixing chamber was designed by considering the effective mixing volume and appropriate mixing mass to ensure uniform blending of milled charcoal with the starch binder prior to moulding.

2.3.1 Determination of the mixing chamber volume

The mixing chamber was designed as a vertical cylindrical drum with the following internal dimensions as shown in Figure 1. The diameter is 0.5 m and height is 0.4 m. The total internal volume of the chamber was determined using Equation 11.

Corresponding author's email address: skishk2009@gmail.com

$$V_{mixer} = \frac{\pi D_{mixer}{}^2 H_{mixer}}{4} \quad 11$$

Where V_{mixer} is the volume of the mixer (m³), D_{mixer} is the diameter of the mixing drum (m), H_{mixer} is the mixer drum height (m).

$$V_{mixer} = \frac{\pi \times (0.50)^2 \times 0.40}{4}$$
$$V_{mixer} = 0.0785 \text{ m}^3$$

During operation, the mixing chamber is not completely filled to allow free movement of material and effective agitation. For batch mixing of granular solids, an effective filling ratio of 70% of the total volume is commonly adopted.

$$V_e = 0.7 V_{mixer}$$

Where V_e is the effective mixing volume (m³).

$$V_e = 0.7 \times 0.0785$$
$$V_e = 0.055 \text{ m}^3$$

2.3.2 Determination of the total mass in mixing chamber

The bulk density of milled charcoal is 200 kg/m³ (as stated by Wasfy and Awny (2020)), The corresponding mass of charcoal in the effective mixing volume was obtained using Equation 12 (Sulaiman *et al*., 2021).

$$m_c = \rho_c V_e \quad 12$$

Where m_c is the mass charcoal (m) and ρ_c is the density of charcoal (kg/m³).

$$m_c = 200 \times 0.055$$
$$m_c = 11.0 \text{ kg}$$

A starch binder content of 5% by mass was adopted as suggested by Lomunyak *et al*. (2024) and Aliero *et al*. (2022), which is typical for briquette production.

$$m_b = 0.05 m_c$$

Where m_b is the binder mass (kg).

$$m_b = 0.55 \text{ kg}.$$

The starch binder is mixed with water to form a slurry. Assuming a binder–water ratio of 1:1 by mass:

$$m_w = 0.55 \text{ kg}$$

where m_w is the mass of water. The total mass of material in the mixing chamber becomes:

$$m_t = m_c + m_b + m_w$$
$$m_t = 11.0 + 0.55 + 0.55$$
$$m_t = 12.1 \text{ kg}$$

2.3.3 Determination of mixing power

The power required for the mixing chamber was determined from the torque developed on the mixing shaft during agitation of the charcoal–binder mixture. The torque was estimated based on the resisting force due to the weight of the mixed material acting at the drum radius.

The resisting force due to the weight of the mixture is given by Equation 13.

$$F_r = m_t g \quad 13$$

where F_r is the resisting force (N).

Corresponding author's email address: skishk2009@gmail.com

$F_r = 12.1 \times 9.81 = 118.7$ N
The torque on the mixing shaft is expressed by Equation 14 (Sulaiman *et al*., 2021).

$$T_{ms} = F_r r_{md} \quad 14$$

where T_{ms} is the torque on the mixer shaft (Nm) and r_{md} is the mixer drum radius (m).

Given the drum diameter of 0.50 m:

$T_{ms} = 118.7 \times 0.25 = 29.7$ Nm
The power required for mixing is given by Equation 15 (Sulaiman *et al*., 2021).

$$P_m = T_{ms}\omega \text{ or } P_m = T_{ms}\frac{2\pi N}{60} \quad 15$$

where P_m is the mixing power (W), ω is the angular velocity (rad/s), N is the rotational speed of the mixer (rpm). For a mixer speed of 44 rpm:

$P_m = \frac{2\pi \times 44 \times 29.7}{60}$=136.9 W

Applying a service factor of 1.5 to account for startup resistance and non-uniform material flow, thus, design mixing power was obtained using Equation 16.

$$P_{dm} = 1.5P_m \quad 16$$

Where P_{dm} is the design mixing power (W).

$P_{dm} = 1.5 \times 136.9 = 205$ W

2.3.4 Determination of the mixing shaft diameter

The diameter of the mixing shaft was determined based on torsional strength. The torsion equation for a solid circular shaft is by Equation 17. (Khurmi and Gupta, 2012).

$$T_{ms} = \frac{\pi \tau {d_{ms}}^3}{16} \quad 17$$

where τ is the allowable shear stress for the shaft material (N/m²), d_{ms} is the shaft diameter (m).

$$d^3 = \frac{16T}{\pi\tau} \quad 18$$

$d^3 = \frac{16 \times 29.7}{\pi \times 40 \times 10^6}$
$d^3 = 3.78 \times 10^{-6}$
$d = 0.0156$ m or 15.6 mm

To account for shock loading, misalignment, and fabrication tolerances, a 20 mm diameter mild steel shaft was selected.

2.4 Determination of Power Requirement for the Machine

The machine consists of two major power consuming units: the hammer mill and the mixing chamber. The total mechanical power required is therefore the sum of the design powers of both units.

The design power for the hammer mill is 0.98 kW while the design power for the mixing chamber is 0.205 kW. The total mechanical power required by the machine is obtained by summing both powers.

$$P_{total} = P_d + P_{dm} \quad 19$$
$P_{total} = 0.98 + 0.205$

Corresponding author's email address: skishk2009@gmail.com

$P_{total} = 1.185$ kW
To account for transmission losses in belts, bearings, and other mechanical components, a service allowance of 20% was included.

$P_{design} = 1.2 \times P_{total}$, $P_{design} = 1.2 \times 1.185$, $P_{design} = 1.42$ kW
Since electric motors are not 100% efficient, motor efficiency must be considered. For small electric motors in the range of 1 to 3 kW, an efficiency of 85% is adopted (Sulaiman *et al*., 2021). The required electrical input power is therefore given by Equation 20.

$$P_{input} = \frac{P_{design}}{\eta} \quad (20)$$

$P_{input} = \frac{1.42}{0.85}$
$P_{input} = 1.67$ kW
The selected motor rating must be greater than the calculated input power to ensure safe and reliable operation. The next standard motor size above 1.67 kW is 2.2 kW.

$P_{motor} = 2.2$ kW or 3 hp
Therefore, a 2.2 kW electric motor was selected to drive the combined hammer mill and mixing units. This rating accommodates efficiency losses, starting torque requirements, intermittent overload, and ensures improved durability and operational reliability of the machine.

2.5 Fabrication of the Machine

The fabrication of the machine was carried out in accordance with the detailed working drawings presented in Figure 1 and the completed assembly is shown in Figure 4. The process followed standard mechanical workshop practices to ensure structural rigidity, dimensional accuracy, and operational reliability suitable for small scale biomass processing applications.

2.5.1 Frame construction

The structural frame was fabricated from mild steel angle bars to provide adequate support for the hammer mill, mixing chamber, and moulding unit. Mild steel was selected due to its weldability, availability, and sufficient strength to withstand operational vibration and static loads.

Angle bars were cut to the specified dimensions using a power hacksaw and assembled on a flat surface to maintain alignment. The members were joined using electric arc welding. Care was taken to ensure perpendicularity of vertical supports and proper levelling of the base to minimize misalignment during operation. After welding, the frame was ground smooth at joint interfaces and inspected for structural integrity before component installation.

2.5.2 Fabrication of the hammer mill section

The grinding chamber was fabricated from mild steel plate rolled into a cylindrical form and welded along the longitudinal seam. End plates were machined to accommodate the shaft and bearing housings.

The rotor shaft, previously designed with a selected diameter of 15 mm, was machined on a lathe to achieve proper bearing seating and pulley mounting surfaces. Hammers fabricated from medium carbon steel were cut to size, drilled, and mounted on the rotor using hardened steel pins to permit free swinging motion during impact.

A perforated steel screen was fabricated and installed beneath the hammer assembly to regulate particle size distribution. The screen was bolted to allow easy replacement during maintenance.

2.5.3 Fabrication of the mixing chamber

The mixing chamber was constructed as a vertical cylindrical drum using 3 mm thick mild steel sheet. The sheet was rolled and welded to form the drum body, after which a circular base plate was welded to the lower end.

Corresponding author's email address: skishk2009@gmail.com

Plate 1: a. Fabrication process of the machine, b. Completed machine

A central mixing shaft of 20 mm diameter was machined and fitted with flat mixing paddles arranged symmetrically to promote uniform agitation of the charcoal binder mixture. The paddles were welded to the shaft at predetermined intervals to ensure effective circulation and reduction of dead zones within the chamber.

The shaft was supported by bearings mounted externally to reduce contamination from the charcoal mixture. A discharge outlet was fabricated at the lower section of the drum and fitted with a manually operated gate to control material flow into the moulding unit. The completed mixing assembly is shown in Plate 1b.

2.5.4 Fabrication of the moulding unit

The moulding unit was fabricated from mild steel plates reinforced with flat bars to withstand compressive loading during briquette formation. Cylindrical mould cavities were machined to ensure dimensional uniformity of the charcoal pellets.

A manually operated compaction mechanism was integrated beneath the mixing chamber to allow direct transfer of blended material into the moulds. The compaction plunger was machined to fit closely within the mould cavity to minimize material leakage and improve pellet density.

2.6 Testing Procedure

2.6.1 Determination of throughput

Performance evaluation of the combined grinding and moulding machine was conducted to determine throughput capacity and briquette dimensional uniformity as shown in Plate 2. For each test, 10 kg of dried charcoal was fed into the hammermill, and the grinding time was recorded. Throughput was calculated using Equation 21.

$$\text{Throughput (kg/h)} = \frac{m_p}{t_g} \times 60 \qquad 21$$

where m_p is the mass processed (kg) and t_g is the grinding time (min).

The milled charcoal was subsequently mixed with starch binder in the mixing chamber and compacted in the moulding unit. Briquette quality was assessed by measuring diameter, height, and mass of randomly selected samples using a vernier calliper and digital balance. Mean values were computed to evaluate dimensional consistency and compaction effectiveness.

2.6.2 Determination of shatter index

The durability of the produced charcoal briquettes was evaluated using the shatter index test. This test determines the ability of briquettes to resist breakage during handling, transportation, and storage. A known

Corresponding author's email address: skishk2009@gmail.com

mass of briquette sample was first weighed and recorded as the initial weight (W_1). Each briquette was then dropped repeatedly from a height of 1.5 m onto a solid steel surface. After the drops, the remaining intact briquette pieces were collected and reweighed to obtain the final weight (W_2). Equation 22 was used to obtain the shatter index as suggested by Abdullahi *et al.* (2023). A higher shatter resistance indicates stronger briquettes with better durability.

$$\text{Shatter index} = \frac{W_1 - W_2}{W_1} \times 100 \quad (22)$$

Where SI is the shatter index, W_1 is the initial weight of briquette before shattering (g) and W_2 is the final weight of briquette after shattering (g)

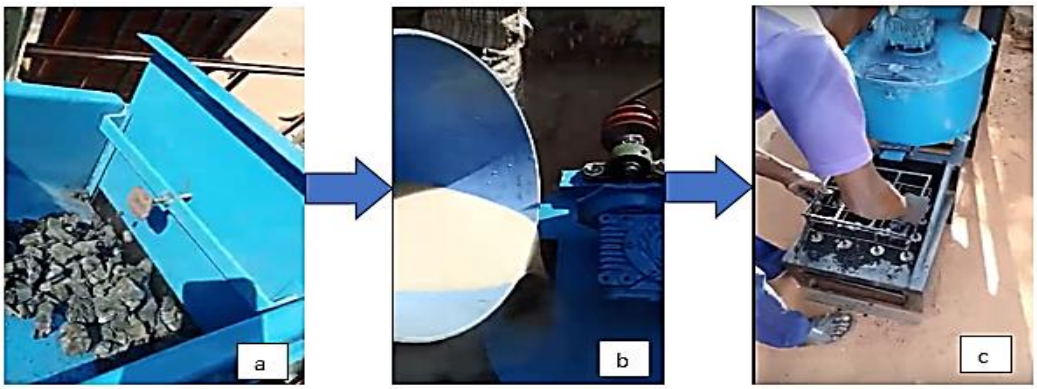

Plate 2: Testing procedure: a. Milling of charcoal, b. Application and mixing of binder, c. Compaction of milled charcoal

2.6.3 Determination of ignition rate

The ignition characteristics of the briquettes were evaluated using the ignition time test. Each briquette sample was marked along its length in mm and ignited at one end using a small flame source. A stopwatch was used to record the time taken for the flame to propagate along the briquette until stable combustion occurred (Abdullahi *et al.*, 2023). The ignition time was determined by measuring the distance burned and the total time taken (Abdullahi *et al.*, 2023).

$$IT = \frac{D}{T} \quad (23)$$

where IT is the ignition rate of flame propagation (mm/min), D is the distance burned (mm) and T is the total time taken (min).

3. Results and Discussion

3.1 Throughput

The grinding tests showed processing times of 12.4, 12.8, and 12.3 min for 10 kg batches as indicated in Table 1, corresponding to throughputs of 48.4, 46.9, and 48.8 kg/h, respectively. The average throughput was 48.0 kg/h, which closely matches the design capacity of 50 kg/h. The small deviation indicates that the selected motor rating and hammer configuration provided sufficient impact energy for effective size reduction without overloading the system. The narrow variation among trials also demonstrates stable and repeatable machine operation.

Table 1: Grinding test results

Test	Mass Processed (kg)	Grinding Time (min)	Throughput (kg/h)
1	10	12.4	48.4
2	10	12.8	46.9
3	10	12.3	48.8
Average	10	12.5	48.0

For capacity/throughput performance of grinding or briquetting machines, the standard metric is:

Corresponding author's email address: skishk2009@gmail.com

$$\text{Efficiency (\%)} = \frac{\text{Actual throughput}}{\text{Design throughput}} \times 100 \quad (24)$$

Using results from Table 1, where actual average throughput is 48.0 kg/h and design is capacity is 50 kg/h. Therefore, the machine capacity efficiency is 96.1%.

This indicates the machine is operating very close to its intended design output, with minimal losses. The results obtained in this study are higher than the efficiencies of 95% and 92.6% reported by Desta and Oumer (2022) and Princewill (2017), respectively. The moulding unit produced briquettes with consistent geometry. All samples maintained a constant diameter of 40 mm, reflecting proper mould cavity design and minimal radial deformation during compaction. The average height and mass were 35 mm and 85 g as presented in Table 2 respectively, with only minor variations between trials. This uniformity suggests adequate mixing of charcoal with the binder and effective pressure transmission within the mould, resulting in structurally stable pellets as shown in Plate 3.

Table 2: Briquette physical properties

Property	Test			Average
	1	2	3	
Diameter (mm)	40	40	40	40
Height (mm)	34	36	35	35
Mass (g)	83	87	85	85

Overall, the close agreement between experimental throughput and design predictions, together with consistent briquette dimensions, confirms that the integrated grinding–mixing–moulding system operates efficiently and meets the intended small-scale production capacity. The results validate the suitability of the machine for continuous and reliable charcoal briquette production.

Plate 3: Pelletised charcoal

3.2 Shatter Index and Ignition Time

The results of the shatter index and ignition rate tests are presented in Table 3. The shatter index values obtained from the three tests were 6.80%, 6.40%, and 7.60%, with a corresponding average value of 6.93%. The relatively small variation among the individual values indicates consistent mechanical performance of the briquettes produced by the machine. The average shatter index of 6.93% suggests that the briquettes possess adequate resistance to breakage. The results are similar to those 6.92% obtained by Abdullahi *et al.* (2023). This mechanical strength can be attributed to effective size reduction during grinding and proper compaction during the moulding process, which improves particle bonding within the briquette structure.

Table 3: Shatter index and ignition rate

S/N	Initial Weight (g)	Final Weight (g)	Shatter Index (%)	Distance Burned (mm)	Time (min)	Ignition Rate (mm/min)
1	100	93.20	6.80	80	9.50	8.42
2	100	93.60	6.40	80	10.50	7.62
3	100	92.40	7.60	80	9.90	8.08
Average	100	93.07	6.93	80	9.97	8.04

Corresponding author's email address: skishk2009@gmail.com

The ignition rate results obtained from the three tests were 8.42, 7.62, and 8.08 mm/min, giving an average value of 8.04 mm/min. The ignition rates show minimal variation, indicating stable combustion characteristics of the produced briquettes. The average ignition rate reflects a steady flame propagation along the briquette, which is desirable for domestic cooking applications that require controlled and sustained heat release. The ignition rates obtained in this study are comparable to the findings of Abdullahi *et al.* (2023) who reported ignition rates between 6 and 9 mm/min for biomass briquettes. However, the values are higher than those reported by Olajide (2010) which ranged between 2 and 5 mm/min. The relatively higher ignition rates observed in the present study may be attributed to improved particle size reduction and compaction during briquette formation, which enhance air penetration and combustion efficiency. Nevertheless, the ignition rates recorded still indicate moderate and controlled burning, which is suitable for domestic applications where longer and stable heat generation is required.

4. Conclusion

A combined charcoal grinding, mixing, and moulding machine was successfully designed, fabricated, and experimentally evaluated for small-scale briquette production. The integrated system effectively reduced charcoal to a uniform particle size, ensured adequate binder mixing, and produced compact briquettes with consistent geometry. Performance testing showed an average throughput of 48.0 kg/h, closely matching the design capacity of 50 kg/h and corresponding to a capacity efficiency of 96.1%, indicating efficient utilization of the installed power and stable grinding performance.

The moulding unit produced briquettes with uniform physical properties, with an average diameter of 40 mm, height of 35 mm, and mass of 85 g, demonstrating effective compaction and proper mould design. Durability evaluation showed an average shatter index of 6.93%, indicating good resistance to breakage during handling and transportation. Combustion evaluation yielded an average ignition rate of 8.04 mm/min, which reflects steady flame propagation and stable combustion behaviour suitable for domestic cooking applications.

Overall, the close agreement between theoretical design predictions and experimental results confirms that the integrated machine operates efficiently and reliably. The developed system therefore provides a practical and affordable solution for converting charcoal fines and agricultural residues into densified fuel for small-scale and rural energy applications.

Acknowledgements

This work was funded by TETFUND–Innovation and Fabrication Grant 2021/2022 Intervention.

References

Abdullahi, M., Enock, OI., Ohiemi, IE. and Samuel, ON. 2023. Production and characterisation of briquette charcoal from carbonised shea nut shell (SNS). *Proceedings of the Susutainable Clean and Emerging Energy Technologies Conference* (pp. 297-305). Nsukka: University of Nigeria.

Adebukola, AA. and Patrick, OA. 2019. Development and evaluation of a fish feed mixer. *AgricEngInt: CIGR Journal*, 21(3): 226-233.

Adejugbe, IT., Olowonubi, JA., Olorunsola, IT., Oyegunwa, OA., Ayeni, JO., Komolafe, O. and Ogunkoya, AK. 2023. Development of a Low-Cost Hammer Mill Machine for Food Processing. *Physical Science International Journal*, 27(3): 16-26.

Adeleke, AA., Ikubanni, PP., Orhadahwe, TA., Christopher, CT., Akano, JM., Agboola, OO., Adegoke, SO., Balogun, AO. and Ibikunle, RA. 2021. Sustainability of multifaceted usage of biomass: A review. *Heliyon*, 7(9): 1-25.

Adetola, OA., Akindinola, BJ. and Sedara, AM. 2022. Development and optimization of double compartments grinding machine for agricultural processes. *Adeleke University Journal of Engineering and Technology*, 5(2): 61-71.

Ajayi, CO., Oyawale, FA. and Afolalu, SA. 2019. Development of blender-hammer mill for multipurpose use. *Journal of Physics: Conference Series*, 1378(2019): 1-8.

Corresponding author's email address: skishk2009@gmail.com

Aliero, YA., Omotosha, GM., Sirajo, A., Sabiyel, AN., Magawata, ZU. and Isa, M. 2022. Effect of cassava starch and tree gum binders on the physical properties of onion leaves briquettes. *International Review of Applied Sciences*, 8(1): 1-9.

Bassey, J., Odesola, I. and Olawuyi, J. 2022. A Comparative Technique for Performance Evaluation of Hammer Mill and Disk Mill in Yam Flour Processing . *World Journal of Engineering and Technology*, 10(3): 613-625.

Budynas, RG. and Nisbett, JK. 2015. *Shigley's Mechanical Engineering Design.* New York: McGraw-Hill Education.

Dermawan, A., Tangkemanda, A., and Muttaqin, AN. 2025. Design and construction of a mixing machine in the process of manufacturing coconut shell charcoal briquettes. *Engineering Proceedings*, 84(1): 28-38.

Desta, MA., and Oumer, A. 2022. Design and Performance Evaluation of Grain Feed Grinding Machine. *Turkish Journal of Agricultural Engineering Research*, 3(2): 231-244.

Gil, M., and Arauzo, I. 2014. Hammer mill operating and biomass physical conditions effects on particle size distribution of solid pulverized biofuels. *Fuel Processing Technology*, 127: 80–87.

Irechukwu, CC., Lawal, SA., Sadiq, IO., Abdullahi, AA., and Abutu, J. 2025. Optimization of fca and mig welding parameters for AISI-1045 steel. *Nigerian Journal of Technology (NIJOTECH)*, 44(4): 576-589.

Khurmi, RS., and Gupta, JK. 2012. *A textbook of machine design.* New Delhi: S. Chand Publishing.

Lackner, M., and Besharati, M. 2025. Agricultural Waste: Challenges and Solutions, a Review. *Waste*, 3(18): 1-32.

Li, C., Bai, Y., Ren, R., Liu, G., and Zhao, J. 2019. Study of the mechanism for improving green pellet performance with compound binders. *Physicochemical Problems of Mineral Processing*, 55(1): 153-162.

Lomunyak, G., Osodo, B., Njoka, F., and Kombe, EY. 2024. Characterization, Optimization and Emission Analysis of Manually-Made Charcoal Dust Briquettes with Starch, Paper and Algae Binders. *Heliyon*, 10(1): 1-14.

Maqsood, S., Navaf, M., Kumar, P., Yucetepe, A., Thuy, NNT., Ozkan, G., Moreno, A., Capanoglu, E., Khalid, W., and Esathbeyoglu, T. 2025. Sustainable utilization of corn waste and their role toward the circular economy. *Journal of Agriculture and Food Research*, 23: 1-25.

Mishra, AK., Ram, S., and Kumar, A. 2017. Design and analysis of spring loaded lift table for industrial application using FEA. *International Journal of Advanced Scientific Research and Management,* 2(5): 65-71.

Mugabi, R., Byaruhanga, YB., Eskrigbe, KM., and Weller, CL. 2019. Performance evaluation of a hammer mill during grinding of maize grains. *AgricEngInt: CIGR Journal*, 21(2): 170-179.

Olajide, JT. 2010. Fuel characterisation and briquettes produced from corncob and rice husk residues. *The Pacific Journal of Science and Technology*, 11(1): 101-106.

Oyelami, A., and Oluwole, A. 2023. Incorporating grain detection and speed control mechanisms in hammer mill operations. *Nigerian Journal of Technology (NIJOTECH)*, 42(2): 222-229.

Princewill, NC. 2017. Development and Performance Evaluation of Improved Hammer Mill . *Journal of Scientific and Engineering Research*, 4(8): 159-164 .

Rhodes, M. 2008. *Introduction to Particle Technology.* US: John Wiley & Sons.

Sithole, T., Pahla, G., Mashifana, T., Mamvura, T., Dragoi, E., Saravanan, A., and Sadeghifar, H. 2023. A review of the combined torrefaction and densification technology as a source of renewable energy. *Alexandria Engineering Journal*, 82: 330-341.

Corresponding author's email address: skishk2009@gmail.com

Sulaiman, I., Egbe, EAP., Abdullahi, M., Saraki, YA. and Shehu, IA. 2021. Design and performance evaluation of a stone crusher. *UNIOSUN Journal of Engineering and Environmental Sciences*, 3(2): 70-77.

Vodounnou, EC., Djossou, AA., Fannou, JL., Semassou, GC. and Ballo, MA. 2022. Study and design of a poultry feed crusher-calibrator. *GSC Advanced Research and Reviews*, 13(3): 24-38.

Wasfy, KI., and Awny, A. 2020. Production of high-quality charcoal briquettes from recycled biomass residues. *Journal of Soil Sciences and Agricultural Engineering*, 11(12): 779-785.

Yan, W., Chen, Z., and Sheng, K. 2015. Carbonization temperature and time improving quality of charcoal briquettes. *Nongye Gongcheng Xuebao/Transactions of the Chinese Society of Agricultural Engineering*, 31(24): 245-249

Corresponding author's email address: skishk2009@gmail.com